Surfaces and Interfaces 41 (2023) 103271

Contents lists available at ScienceDirect

Surfaces and Interfaces

journal homepage: www.sciencedirect.com/journal/surfaces-and-interfaces

The role of surface thermodynamics and kinetics in the removal of PFOA from aqueous solutions

Mengru Zhang [a], François Sicard [a], Turan Selman Erkal [a], Geoffrey M. Bowers [b], A. Ozgur Yazaydin [a,*]

[a] Department of Chemical Engineering, University College London, London WC1E 7JE, United Kingdom
[b] Department of Chemistry and Biochemistry, St. Mary's College of Maryland, St. Mary's City, MD 20686, United States

ARTICLE INFO

Keywords:
Perfluorooctanoic acid
All-silica zeolites
Interfacial adsorption
Adsorption kinetics
Molecular dynamics

ABSTRACT

Perfluorooctanoic acid (PFOA) has been extensively used as surfactant in industrial applications. Human exposure to PFOA through contaminated water has been linked to serious adverse health effects. In this work, the removal of PFOA from water in all-silica zeolites, which are hydrophobic materials with diverse pore geometries and exceptional hydrothermal stability, is studied. Molecular scale structure, dynamics, kinetics, and free energy landscapes associated with PFOA adsorption are characterized. Interfacial adsorption constitutes the rate limiting step and the adsorption of PFOA is orientation competitive. The PFOA orientation where the hydrophobic perfluorinated methyl group is adsorbed first on the zeolite surface is thermodynamically favored; whereas the adsorption kinetics is faster when the hydrophilic carboxyl group is adsorbed first. Furthermore, the adsorption of PFOA in deprotonated state in hydrophobic pores is thermodynamically prohibitive. Based on computed permeabilities in the pores and kinetic rates associated with the adsorption of PFOA from water, three zeolites, MTW, VET and GON, are estimated to exhibit several orders of magnitude better PFOA removal performance compared to the benchmark material, zeolite Beta (BEA).

1. Introduction

Perfluorooctanoic acid (PFOA) is an anthropogenic perfluorinated alkyl substance (PFAS) that has been widely used as surfactant in fire retardants, polymer synthesis, paper coatings, and fabric protection due to its unique amphiphilic structure made of a hydrophilic carboxyl group head and a hydrophobic perfluorinated tail [1–4]. The large C-F bond energy, which is around 440 kJ·mol^{-1}, provides PFOA with a high chemical stability while the carboxyl group makes it soluble in water (3400 mg·L^{-1}) [5,6]. The release of PFOA to the environment as a result of its widespread use has raised concerns due to PFOA's non-degradability in nature and its consequent accumulation in animals, humans and aquatic environments. PFOA exposure has been linked to adverse health effects in humans, including increased risk of kidney and testicular cancer, immunosuppression, reproductive toxicity, cardiovascular, respiratory and neurological diseases [7–15]. Noteworthily, it was shown that PFOA is transferred to fetuses in pregnant women, which can lead to birth defects [16,17]. Although some countries have formulated laws and regulations to limit or forbid PFOA usage, it is still irreplaceable in many industries and not expressly restricted in most countries, leading to continued and widespread pollution [18,19]. For example, PFOA has been detected in seals, cods, and zooplankton of the Arctic region in Canada far from any point sources of this pollutant [20]. Therefore, it is crucial to separate and remove PFOA from the environment and its selective capture from natural water remains a daunting challenge given that it is present in very low concentrations in natural waters.

Various methods have been used for PFOA removal from water, such as bioremediation, photodegradation, coagulation, ultrasonic degradation, and adsorption [21–27]. Among them, adsorption by porous materials is as a low cost, easy to operate, and environmentally friendly PFOA removal technology [21,23]. Zeolites, which are inorganic crystalline porous materials, have received interest as potential adsorbents for PFOA removal in water treatment due to their preferable characteristics of diverse pore geometries and sizes, and exceptional hydrothermal stability [28–33]. For instance, Na-exchanged Y zeolites were employed as PFOA adsorbent, and it was reported that a higher Si/Al ratio provided NaY zeolites with better adsorption performance [28].

* Corresponding author.
E-mail address: ozgur.yazaydin@ucl.ac.uk (A.O. Yazaydin).

https://doi.org/10.1016/j.surfin.2023.103271
Received 7 July 2023; Received in revised form 27 July 2023; Accepted 9 August 2023
Available online 12 August 2023

Silver-exchanged FAU-type zeolite demonstrated improved performance for PFOA adsorption due to specific extra adsorption sites after being functionalized with 3-aminopropyltriethoxy at the external surface [31]. Van den Bergh et al. experimentally demonstrated the use of all-silica zeolite Beta (BEA) as a highly selective adsorbent for the removal of PFOA from water [32]. They showed that all-silica BEA was more effective than activated carbon for the removal of PFOA, and that the PFOA uptake decreased significantly with decreasing Si/Al ratio as well as increasing number of silanol defects, both of which make BEA less hydrophobic. In the same study, it was highlighted that the possibility of thermal generation is a significant asset for all-silica BEA, because such a simple treatment cannot be applied for organic adsorbents like macrocyclic polymers or ion-exchange resins.

In this study, zeolite topologies in their all-silica form were investigated to determine their potential for PFOA removal from water. Monte Carlo (MC) and molecular dynamics (MD) simulations were performed to characterize the pore limiting diameter (PLD) and largest cavity diameter (LCD) of 237 all-silica zeolites and their associated PFOA Henry coefficient, diffusion coefficient and ideal permeability coefficient as well as the hydrophobicity of zeolites. Based on the MC and MD simulations MTW, VET and GON topologies were identified as the most promising zeolite structures. Crucially, we carried out free energy (FE) calculations to understand the adsorption mechanism of a single PFOA molecule from water in these zeolites with a focus on the thermodynamics and kinetics of the interfacial adsorption process, which are often overlooked in molecular scale studies of adsorption. In the literature, several enhanced sampling techniques have been developed to explore the free energy landscapes of the conformational space within accessible simulation time scales, such as umbrella sampling (US) [34], metadynamics [35], steered MD [36] and adaptive biasing force methods [37]. Among them, US, combined with the weighted histogram analysis (WHAM), has been extensively used to study adsorption processes [38–41]. By carrying out US calculations, we computed the FE landscapes associated with the adsorption of PFOA from water in MTW, VET and GON all-silica zeolites. The results for these zeolites were compared with those for BEA, which was used as the benchmark zeolite in our study due to its successful experimental utilization for PFOA removal from water [32].

2. Computational methods

In this section, we provide a summary of the computational methods used. Detailed explanation of the models and methods can be found in the SI.

2.1. All-silica zeolite, PFOA and water models

All-silica zeolite topologies were constructed based on their crystallographically determined structures as described in the International Zeolite Association Structure Commission (IZA-SC) database [42]. PLDs and LCDs of the zeolite structures were computed with the Poreblazer v4.0 code [43]. The united-atom TraPPE and OPLS-AA force fields were employed to model the perfluoroalkyl group and carboxyl group of PFOA, respectively [44–47]. In this model, which was used in a recent study [48], $–CF_3$ and $–CF_2$ groups are represented as united-atoms. The SPC/E water model was used to represent the water molecules [49].

2.2. Monte Carlo simulations

MC simulations were carried out to calculate the Henry coefficients (H_C) of PFOA and water to characterize the PFOA affinity and hydrophobicity of zeolites, rescpectively. Henry coefficient of a molecule in a zeolite can be computed by Widom's insertion method

$$H_C = \lim_{b_i \to 0} \frac{\beta}{\rho_{zeo}} \frac{\langle W \rangle}{\langle W^{IG} \rangle} \tag{1}$$

where ρ_{zeo} is the density of the zeolite, $\beta = 1/(k_B T)$, $k_B$is the Boltzmann constant, T is the temperature, $\langle W \rangle$ is Rosenbluth weight, and $\langle W^{IG} \rangle$ is the ideal Rosenbluth weight of a single molecule in the ideal gas phase [50]. It should be noted that H_C corresponds to the reciprocal of the Henry's Law constant which is defined as, $K_H = \lim_{b_i \to 0} \frac{f_i}{b_i}$, where $b_i$and $f_i$are molality and fugacity of adsorbate i, respectively. Henry coefficients of PFOA and water in zeolites were computed by sampling 10^5 and 5×10^6 random Widom's particle insertions for H_2O and PFOA, respectively, using the RASPA molecular simulation software [51–53].

2.3. Molecular dynamics simulations

MD simulations were implemented to calculate the self-diffusion coefficient (D_i) and FE landscapes. D_i is obtained by linear regression of the mean square displacement (MSD) computed from MD simulations according to the Einstein's relation [54,55]:

$$D_i = \frac{1}{2d} \frac{\left\langle (\boldsymbol{r}(t) - \boldsymbol{r}(0))^2 \right\rangle}{t} \tag{2}$$

where t is time, r(t) is the position of the particle at any given time, r(0) is the particle's initial position, and d is 1, 2 or 3 depending on the pore dimensionality of the adsorbent material, i.e., 1D, 2D, or 3D, respectively. Self-diffusion coefficients of PFOA at infinite dilution; i.e. single molecule, were computed by carrying out MD simulations in the NVT ensemble at 298.15 K for 300 ns using a Nose-Hoover thermostat [56]. The MSDs of the PFOA molecule were obtained by averaging the trajectories of 30 independent MD simulations in each zeolite (**Figs. S8–S10**).

FE landscapes associated with the adsorption of PFOA from water in zeolites were computed by carrying out US simulations. Fig. 1 shows the setup used for the US simulations. The adsorption coordinate represents the distance between the center of mass (COM) of a single PFOA molecule and the COM of the zeolite along the straight channels, i.e., in the direction of the z-coordinate. Two different orientations of PFOA, the hydrophobic $–CF_3$ group facing the zeolite surface (Orientation I, Fig. 1**b**), and the hydrophilic –COOH group facing the zeolite surface (Orientation II, Fig. 1**c**), were considered for the US calculations. A series of 90 configurations was evenly generated along the z direction within the range [0, 9] nm by using a steering simulation with the pull rate 0.01 nm ps^{-1}. During both pulling and US simulations, the harmonic spring constant $\boldsymbol{k_i}$ was set to 1000 kJ mol^{-1} nm^{-2}. All MD simulations and US calculations were performed using the GROMACS simulation package (version 2019.3) [57].

3. Results and discussion

3.1. Computational screening of zeolites

Given that the recognized size of PFOA molecule is ~5 Å, zeolites with a smaller PLD are not expected to adsorb PFOA. Here, we considered a PLD threshold of 4 Å, which allowed us to eliminate 136 of the zeolites (Fig. 2). For the remaining 101 all-silica zeolite topologies, water and PFOA Henry coefficients were computed.

The *pKa* values of PFOA reported by experimental studies vary between 0.5 and 3.8 [58–62], therefore, PFOA is expected to be in the deprotonated state in hydrophilic environments due to presence of liquid water; i.e. $pH = 7$. Consequently, molecular simulation studies investigating the adsorption of PFOA in hydrophilic materials, such as clay minerals [63,64] and cyclodextrin-based polymers [65], employed deprotonated models of PFOA. In contrast, PFOA is expected to be in neutral state when water is not present, i.e., near hydrophobic surfaces. Therefore, we used a neutral model for the PFOA molecule in our study because water is not anticipated to enter the hydrophobic pores of all-silica zeolites (See SI for the details of the neutral PFOA model). We

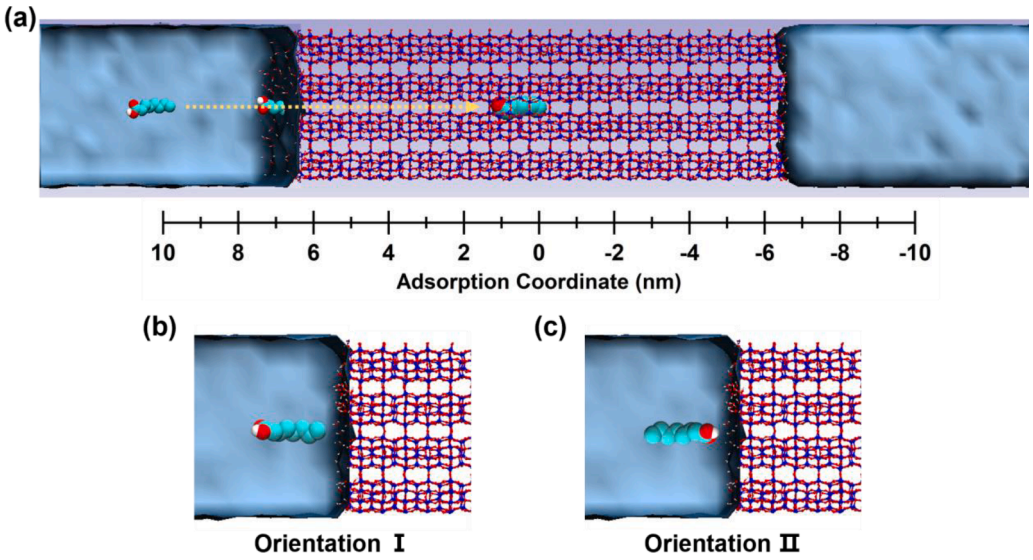

Fig. 1. (a) Setup for US calculation of a single PFOA molecule adsorption from water (light blue regions) into zeolites. The yellow dashed line represents the reaction coordinate sampled, which runs in the z-direction. Two different orientations of PFOA considered are shown in (b) Orientation I, the hydrophobic $–CF_3$ group facing the zeolite surface; and (c) Orientation II, the hydrophilic –COOH group facing the zeolite surface. Color scheme: O, red; Si, dark blue; $–CF_x$, bright blue, H, white.

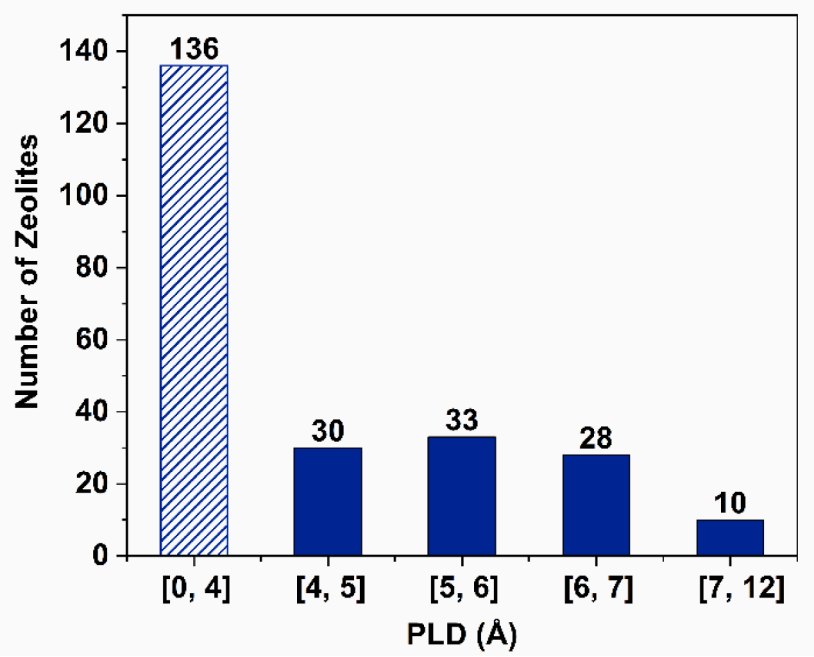

Fig. 2. Distribution of zeolites with respect to computed PLDs.

justify the use of a neutral PFOA model in Section 3.4., by presenting comparative free energy analyses of the adsorption of PFOA in neutral and deprotonated states, which show that the presence of PFOA in deprotonated state in the hydrophobic pores of an all-silica zeolite is thermodynamically prohibitive. Indeed, the computed Henry coefficients of water in all-silica zeolites were all below 1.0×10^{-6} $mol{\cdot}kg^{-1}{\cdot}Pa^{-1}$, which is a consequence of their significant hydrophobicity. Whereas the computed PFOA Henry coefficients in all-silica zeolites ranged from 10° to 10^{7} $mol{\cdot}kg^{-1}{\cdot}Pa^{-1}$, which are significantly larger than the water Henry coefficients (Fig. 3). These results indicate that some all-silica zeolites can be used for the removal of PFOA at very low concentrations in water because of their high PFOA affinity and very high hydrophobicity. Fig. 3 shows a scatter of PLDs versus LCDs for 101 all-silica zeolites with PFOA Henry coefficients. From the perspective of pore size, all-silica zeolites with PLDs and LCDs in the range of 5.0 to 7.0 Å, in general, have larger PFOA Henry coefficients (purple area in Fig. 3) compared with all-silica zeolites with PLDs and LCDs within the range of 7.0 to 12.0 Å. This is because in larger pores, the interaction between PFOA and the zeolite framework is weaker.

There are 55 zeolites topologies with PFOA Henry coefficient values above 10^{4} $mol{\cdot}kg^{-1}{\cdot}Pa^{-1}$, however, among them, 31 zeolite topologies have been synthesized experimentally in the siliceous form, which are represented by the closed symbols in Fig. 3, whereas open symbols represent the zeolite topologies for which the all-silica synthesis have not been reported. It is well known that defects in zeolites are preferred adsorption sites for water, and zeolites with defects are not anticipated to capture PFOA from water effectively. Herein, we only considered the 25 zeolite topologies with computed PFOA Henry coefficients above 1.0

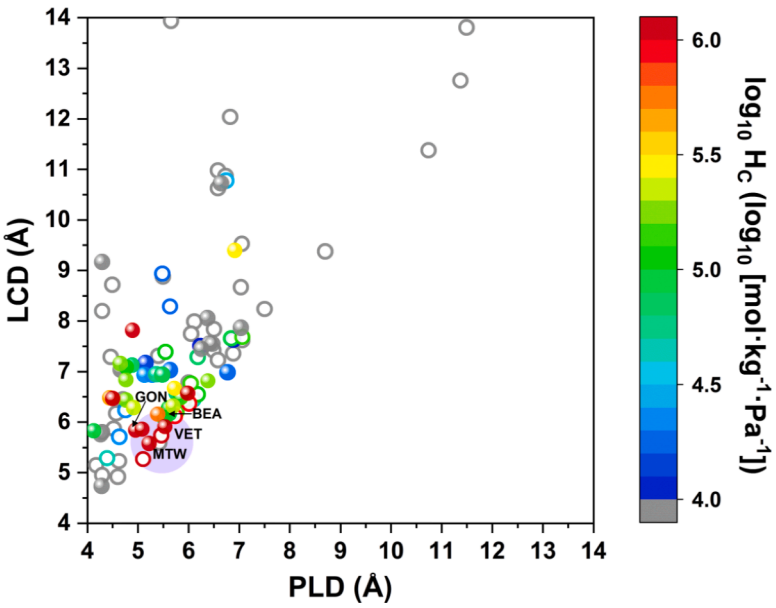

Fig. 3. 2D Color-mapped scatter plot of the logarithm of the computed PFOA Henry coefficients ($\log_{10}$ H_C) versus the computed PLDs versus LCDs for 101 all-silica zeolites. Filled circles represent zeolites that have been synthesized in all-silica form. Open circles represent zeolites that have not been synthesized in all-silica form yet. The all-silica zeolites with LCDs and PLDs in the range [5.0, 6.0] Å, such as MTW, VET, GON, as circled in the purple area, possess the largest PFOA Henry coefficients among others.

$\times 10^4$ mol·kg^{-1}·Pa^{-1} (Tables S2–S5) and for which all-silica synthesis were reported.

To further evaluate the PFOA removal performance of the 25 all-silica zeolite topologies, their ideal permeability coefficients (π_i) based on the solution-diffusion model were computed [66]. According to this model, $\pi_i = K_i \times D_i$, where K_i and D_i are the solubility coefficient and the self-diffusion coefficient, respectively, of PFOA in all-silica zeolites [67]. The solubility coefficient can be represented by the Henry coefficient at low loadings. The use of ideal permeability is justified by the fact that water does not enter hydrophobic zeolite pores, so the PFOA molecule only interacts with the zeolite framework. The final 25 all-silica zeolite topologies were classified into three categories based on their pore dimensionality and the computed PFOA diffusion coefficients are presented in Tables S3–S5. In general, computed PFOA diffusion coefficients are largest in zeolites with 1D pores, followed by zeolites with 2D and 3D pores. This is because molecules spend longer times at the intersection of the pores in zeolites with 2D and 3D pores, resulting in smaller self-diffusion coefficients.

Based on their optimum pore size, high PFOA affinity, fast PFOA diffusion and the computed PFOA ideal permeabilities, MTW, VET, and GON emerged as the most promising zeolites for PFOA removal from water. In Table 1, their ideal permeabilities are given in comparison to BEA. Noteworthily, MTW, VET, and GON are all zeolites 1D pores, while BEA has 2D pores. MTW shows the largest ideal PFOA permeability coefficient, which is four orders of magnitude larger than that of BEA, followed by VET and GON with their ideal PFOA permeability coefficients four and three orders of magnitude larger than that of BEA, respectively.

Table 1
Comparison of the computed properties of MTW, VET and GON with BEA.

	PLD (Å)	LCD (Å)	PFOA Henry coefficient (mol·kg^{-1}·Pa^{-1})	PFOA self-diffusion coefficient (cm^2·s^{-1})	PFOA ideal permeability coefficient (cm^2·mol·kg^{-1}·Pa^{-1} s^{-1})
MTW	5.22	5.58	2.83×10^6	1.47×10^{-2}	4.16×10^4
VET	5.53	5.91	1.74×10^6	6.24×10^{-3}	1.09×10^4
GON	4.95	5.84	1.05×10^6	2.18×10^{-3}	2.29×10^3
BEA	5.62	6.17	9.81×10^4	1.18×10^{-5}	$1.16 \times 10^{\circ}$

3.2. Free energy analyses

To understand the thermodynamics of the PFOA adsorption process, we performed US calculations (see SI for details) and characterized the FE landscapes of a single PFOA molecule adsorbed from water in MTW, VET, GON and BEA, for two orientations of PFOA; the hydrophobic –CF_3 group facing the zeolite surface (Orientation I), and the hydrophilic –COOH group facing the zeolite surface (Orientation II). The corresponding FE profiles, as a function of the adsorption coordinate, for BEA is shown in Fig. 4**a** and for MTW, VET, GON are shown in Fig. 5. The channels of the MTW, VET, GON and BEA all-silica zeolites which run in the direction of the PFOA adsorption coordinate sampled in the US calculations are shown in **Fig. S2**.

For Orientation I, the FE profiles of the zeolites can be divided into four parts with respect to maximum point A, minimum B, and local maximum C, as illustrated in Fig. 4**a** for BEA. Before point A, the PFOA molecule stays in water and the FE of the adsorption system is regarded as 0 kJ mol^{-1}. The other three parts constitute the adsorption process, namely Stage I, II, and III as illustrated in Fig. 4**b**. Each stage is characterized by ΔG^I_{sur}, ΔG^I_{int}, and ΔG^I_{por} (Fig. 4**a**), which are defined as the free energy of surface adsorption, interfacial barrier, and pore-structural barrier, respectively. By comparison, there is no Stage II (from B to C) in the FE profiles of all the four target zeolites for Orientation II. Therefore, the adsorption process of Orientation II comprises 2 stages, Stage I and III (Fig. 4**c**), which are quantified by ΔG^{II}_{sur} and ΔG^{II}_{por}, respectively. The free energy of the overall PFOA adsorption process, ΔG_{ads}, for Orientation I and Orientation II are defined as the difference between points A and C in Fig. 4**a**. The ΔG values for the different stages of PFOA adsorption for the four all-silica zeolites are given in Table 2. The large negative ΔG_{ads} values show that the PFOA adsorption process is thermodynamically strongly favoured. While there are no experimental data for MTW, VET and GON zeolites, all-silica BEA was experimentally shown to be effective in removing PFOA from water [32], which is in line with our calculations. In the following sections, we present a detailed analysis of different stages of PFOA adsorption for Orientation I and Orientation II based on free energy profiles.

3.2.1. Orientation I (–CF_3 pore-facing)

The PFOA adsorption in Orientation I has three stages (Stage I, II and

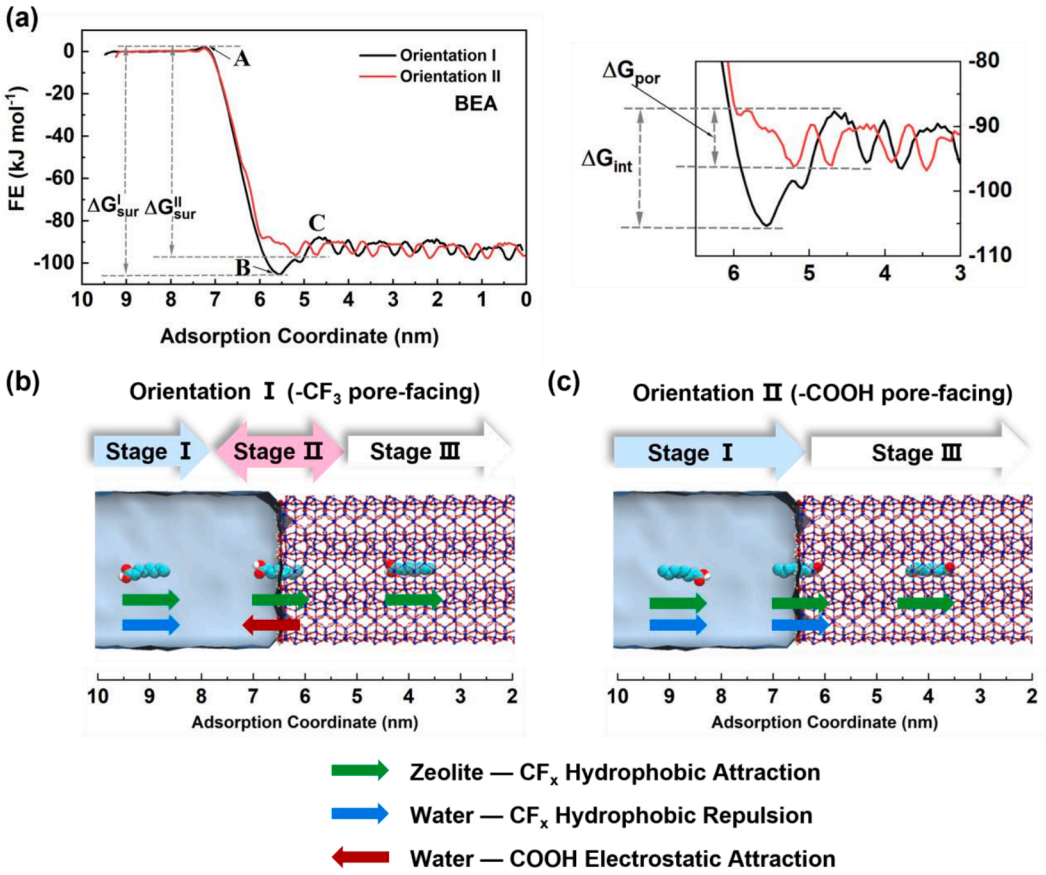

Fig. 4. (a) The free energy (FE) profiles of PFOA adsorption from water into BEA for Orientation I (–CF_3 pore-facing) and Orientation II (–COOH pore-facing). The figure on the right is the enlarged view near the water-zeolite surface. Illustration of the forces at play during different stages of PFOA adsorption from water (light blue regions) for (b) Orientation I (–CF_3 pore-facing) and (c) Orientation II (–COOH pore-facing). Color scheme: O, red; Si, dark blue; –CF_x, bright blue, H, white.

III) as illustrated in Fig. 4**b**. In Stage I, PFOA molecule is adsorbed from bulk water onto the zeolite surface. The free energy change in this stage (ΔG^I_{sur}) exhibits a significant decrease in the free energy profile between the reference point A and the FE minimum, point B, as illustrated in Fig. 4**a**. At the FE minimum point, there are competing effects of the hydrophobic repulsion between water and the perfluorinated chain of PFOA and the hydrophobic attraction between all-silica zeolite and the perfluorinated chain of PFOA. ΔG^I_{sur} for VET and GON are similar and ~ 7.0 kJ mol^{-1} lower than that of benchmark BEA, while ΔG^I_{sur} of MTW is ~ 11 kJ mol^{-1} higher, suggesting that PFOA would be more strongly adsorbed on the surface of the VET and GON compared to the BEA.

In Stage II, PFOA must overcome the interfacial free energy barrier, ΔG^I_{int}, which vary from 13.7 to 17.6 kJ mol^{-1} depending on the zeolite framework (Table 2). The interfacial energy barrier is mainly due to two competing interactions; electrostatic attraction between water and PFOA carboxyl group and the hydrophobic attraction between all-silica zeolite and the perfluorinated chain of PFOA, which are illustrated with red and green arrows, respectively, in Fig. 4**b**. ΔG^I_{int} values for MTW, VET and GON are all smaller by at least ~ 3.0 kJ mol^{-1} than the one for BEA (17.6 kJ mol^{-1}), demonstrating that it is easier for PFOA to overcome the energy barrier of water/zeolite interface in MTW, VET and GON compared to BEA.

In Stage III, PFOA translocate from the interface to the center of the zeolite by overcoming energy barrier due to the pore structure of zeolites (ΔG^I_{por}). The value of ΔG^I_{por} for BEA is 6.1 kJ mol^{-1}. In comparison, the values of ΔG^I_{por} for MTW, VET and GON are all below 5.0 kJ mol^{-1}, suggesting that it is thermodynamically easier for PFOA to diffuse through the pores of MTW, VET and GON compared to BEA, which is in line with the PFOA diffusion coefficients computed from MD simulations for these four zeolites (Table 1).

3.2.2. *Orientation II (–COOH pore-facing)*

The adsorption of PFOA in Orientation II is characterized by 2 stages (Stage I and III, Fig. 4**c**) and quantified by ΔG^{II}_{sur} and ΔG^{II}_{por}, respectively. There is no Stage II in the FE profiles for this orientation, because when PFOA is in Orientation II it does not experience any significant interfacial energy barrier. This is because the carboxyl group of PFOA does not interact with water at the interface in Orientation II as illustrated in Fig. 4**c**. Therefore, after being adsorbed from bulk water on to the zeolite surface, PFOA must overcome only the energy barrier due to pore structure. At this point, the values of ΔG^{II}_{por} are almost the same as that of ΔG^I_{por} for BEA, VET and GON, except MTW, which exhibits a ΔG^{II}_{por} of 2.3 kJ mol^{-1}, which is ~ half that of ΔG^I_{por} for this zeolite topology. Although the FE minimum (B) of Orientation I at the interface is more negative than that of Orientation II, the FE profiles of Orientation II after Point B are lower than that of Orientation I for VET, GON, and MTW. This may be explained by the fact that at the interface the electrostatic attraction between water and the carboxyl group of PFOA for Orientation I disappears, and the diffusion of PFOA molecule into the zeolite pores is driven by hydrophobic repulsion between water and the perfluorinated chain of PFOA (blue arrow in Fig. 4**c**) and the hydrophobic attraction between the all-silica zeolite and the perfluorinated chain of PFOA (green arrow in Fig. 4**c**).

For the four zeolites considered in Table 2, the values of ΔG^I_{sur} and ΔG^{II}_{sur} are below −90 kJ mol^{-1} regardless of the PFOA orientation, but the values of ΔG^I_{sur} of the four zeolites are more negative than that of ΔG^{II}_{sur}, which is particularly the case for BEA, since the difference between ΔG^I_{sur} and ΔG^{II}_{sur} is significant, i.e., 9.3 kJ mol^{-1}. To quantify the

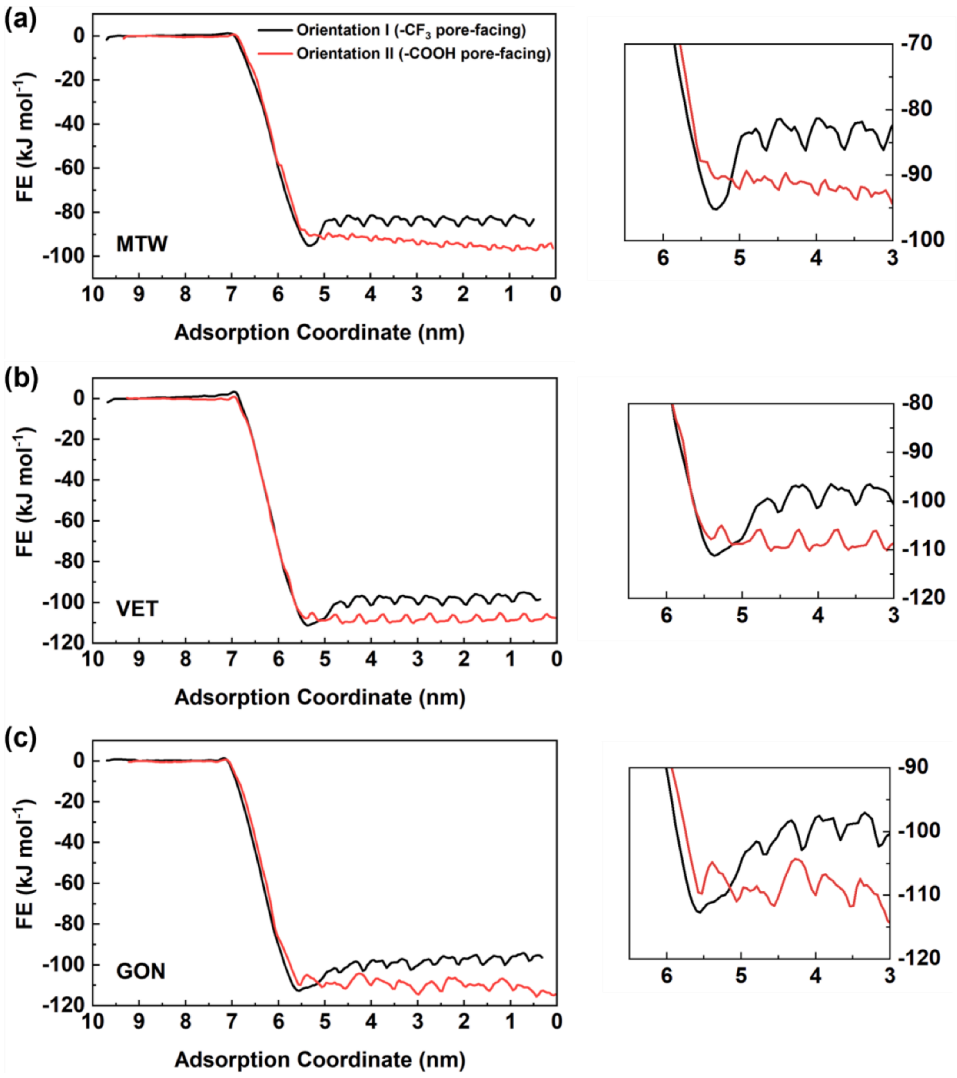

Fig. 5. Free energy (FE) profiles of PFOA adsorption from water in to (a) MTW, (b) VET and (c) GON for Orientation I (–CF_3 pore-facing) and Orientation II (–COOH pore-facing). The figures on the right are the enlarged views around the water-zeolite interface.

Table 2
Summary of free energies associated with PFOA adsorption from water in MTW, VET and GON zeolites in comparison with zeolite BEA.

All-silica zeolites	Orientation I (–CF_3 pore-facing) (kJ mol^{-1})				Orientation II (–COOH pore-facing) (kJ mol^{-1})			
	ΔG^{I}_{sur}	ΔG^{I}_{int}	ΔG^{I}_{por}	ΔG^{I}_{ads}	ΔG^{II}_{sur}	ΔG^{II}_{int}	ΔG^{II}_{por}	ΔG^{II}_{ads}
BEA	−107.2	17.6	6.1	−89.6	−97.9	—	6.4	−91.5
MTW	−96.5	13.7	4.5	−82.8	−93.0	—	2.3	−90.7
VET	−114.7	14.6	4.7	−100.1	−111.2	—	4.1	−107.1
GON	−114.1	14.3	4.9	−99.8	−112.2	—	4.8	−107.4

probabilities of PFOA molecule being adsorbed on the surface in Orientation I and Orientation II, based on Boltzmann distribution theory, one can obtain the ratio of the probabilities of two states (i, j) of the system, which is known as the Boltzmann factor, using:

$$\frac{p_{i(r)}}{p_{j(r)}} = \exp\left(-\left(\Delta G_i - \Delta G_j\right)/RT\right) \quad (3)$$

Accordingly, we computed the ratios of the probability of PFOA being adsorbed on the surface in Orientation I or II (p^{I}_{sur}/p^{II}_{sur}) for MTW, VET, GON and BEA by using the corresponding ΔG^{I}_{sur} and ΔG^{II}_{sur} values given in Table 2. The probability of PFOA adsorption in Orientation I on to the surface of BEA is ~ 43 times larger than in Orientation II, which demonstrates that PFOA is almost certainly adsorbed on to the BEA

Table 3
The ratios of the probability of PFOA being adsorbed on the surface in Orientation I or II (p^{I}_{sur}/p^{II}_{sur})* and rate constants for the rate limiting stages associated with PFOA adsorption from water in MTW, VET and GON zeolites in comparison with zeolite BEA.

	BEA	MTW	VET	GON
p^{I}_{sur}/p^{II}_{sur}	42.6	4.1	4.1	2.2
$k^{I}_{sl,\ PF}$ (× 10^{10} s^{-1})	0.5	2.5	1.7	1.9
$k^{II}_{sl,PF}$ (× 10^{10} s^{-1})	47	245.5	118.8	89.5

* I and II represent Orientation I (–CF_3 pore-facing) and Orientation II (–COOH pore-facing), respectively.

surface in Orientation I, i.e., 97% of the PFOA molecules adsorbed on the surface (Table 3). However, for the three other zeolites the scenario is different. For MTW and VET $p^{I}_{sur}/p^{II}_{sur} = 4.1$ and for GON $p^{I}_{sur}/p^{II}_{sur} = 2.2$, which suggests that, although PFOA adsorption on the surfaces of these three zeolites are still more likely to occur in Orientation I, the probability of surface adsorption of PFOA in Orientation II is significant, such that around 20% and 31% PFOA molecules adsorbed on the surfaces of MTW and VET and surface of GON, respectively, are in Orientation II.

3.3. Kinetics of PFOA adsorption

After being adsorbed from water onto the surface (Stage I), PFOA with Orientation I (–CF_3 group pore-facing orientation) must overcome the interfacial free energy barrier (Stage II) and pore structural energy barrier (Stage III) before being fully adsorbed in the zeolite. To determine the rate constants associated with different stages of PFOA adsorption from water into the zeolite, we used the Eyring equation [68] based on the transition state theory

$$k^{*}_{PF} = \frac{\kappa k_B T}{h} \exp\left(-\frac{\Delta G^{*}}{RT}\right) \quad (4)$$

where k^{*}_{PF} is the rate constant for PFOA adsorption; ΔG^{*} is the free energy barrier; κ is the transmission coefficient, which is 1 [69]; and h is Planck's constant. The computed ΔG values for different stages of the adsorption process from US calculations (Table 2), are used in Eq. (4) to calculate the associated rate constants and are presented in Table 3. The Eyring equation suggests that larger values of free energy barrier lead to lower rate constants, hence slower adsorption kinetics. Since the values of the interfacial free energy barrier (ΔG^{I}_{int}) are significantly larger than that of pore structural energy barrier (ΔG^{I}_{por}), Stage II, which is related to the interfacial free energy barrier, is considered to be the rate-determining step for Orientation I. From the perspective of Orientation II, there is only the pore structural energy barrier (ΔG^{II}_{por}), that is, the rate-determining step for Orientation II is Stage III.

Accordingly, we can compute the slowest rate constants for Orientation I, $k^{I}_{sl,\ PF}$, and Orientation II, $k^{II}_{sl,PF}$, using ΔG^{I}_{int} and ΔG^{II}_{por}, respectively. From the perspective of Orientation I, the value of $k^{I}_{sl,PF}$ for MTW is the largest at $2.5 \times 10^{10}\ s^{-1}$, which is 5 times larger than that of $k^{I}_{sl,PF}$ for BEA; while the values of $k^{I}_{sl,PF}$ for VET and GON are ~ 3 and 4 times larger than that of $k^{I}_{sl,PF}$ for BEA. This means the kinetics of interfacial PFOA adsorption of MTW, VET and GON are faster than that of BEA for Orientation I. From the perspective of Orientation II, the value of $k^{II}_{sl,PF}$ for MTW, VET and GON is ~ 5, 3 and 2 times larger than that of $k^{II}_{sl,PF}$ for BEA, respectively.

As discussed above, the probability analyses of Stage I (adsorption of PFOA from water on to the zeolite surface) shows that PFOA adsorption on the surfaces in Orientation I is thermodynamically more favorable than Orientation II. After Stage I, however, the kinetic rate analyses suggest that PFOA adsorption in Orientation II is faster than Orientation I, i.e., the values of $k^{II}_{sl,PF}$ are ~ two orders of magnitude larger than that of $k^{I}_{sl,PF}$. That is, what we observe is orientation dependent competitive adsorption of PFOA where thermodynamics favor Orientation I and kinetics favor Orientation II. Overall, the PFOA adsorption process is expected to be much faster in MTW, VET and GON since the occurrence of PFOA adsorption in Orientation II on the surface of these three zeolites are significantly more probable compared to BEA.

3.4. The protonation state of PFOA near the surface and in the pores of hydrophobic zeolite

As we mentioned earlier, we employed a neutral PFOA model in our study considering that no water adsorption is anticipated in the hydrophobic pores of all-silica zeolites. However, in pure water, i.e., pH = 7, PFOA is deprotonated. As such, we carried out US calculations of PFOA adsorption in zeolite BEA with a deprotonated PFOA model (See SI for the details of the deprotonated PFOA model) to compare the FE profiles of the deprotonated and neutral PFOA models. The simulation set up for the US calculations with the deprotonated PFOA model were identical to those with the neutral PFOA model except that a single Na^{+} ion was placed in bulk water to make the overall system neutral, since the deprotonated PFOA molecule is negatively charged. Like we did in the case of the neutral PFOA model, we computed the FE landscapes for two PFOA orientations: Orientation I, –CF_3 group facing the zeolite surface, and Orientation II, –COO^{-} group facing the zeolite surface. The corresponding FE profiles of the deprotonated PFOA model as a function of adsorption coordinate are shown in Fig. 6 in comparison with the data for the neutral PFOA model. For both orientations, the FE profiles of the deprotonated PFOA model, shown with dotted lines in Fig. 6, exhibit very large interfacial energy barriers, i.e., > 120 kJ mol^{-1}. That is, it is thermodynamically prohibitive for deprotonated PFOA to be adsorbed inside the hydrophobic pores of all-silica zeolite BEA. Hence, our use of a neutral PFOA model for the initial screening calculations of Henry and self-diffusion coefficients is fully justified. To understand the entire PFOA adsorption process, however, the results obtained with the neutral and deprotonated PFOA models should be interpreted together. The energy minima of the –COO^{-} pore-facing orientation of the deprotonated PFOA near the surface of zeolite BEA, which is located around 6 nm on the adsorption coordinate, is higher, i.e., less negative, than that for the –CF_3 pore-facing orientation. That is, the PFOA molecule is more likely to be adsorbed onto the zeolite surface from water in –CF_3 pore-facing orientation in deprotonated state. The PFOA molecule should then transition from the deprotonated state to the neutral state at the water/zeolite interface to be fully adsorbed in the hydrophobic zeolite pores, where it exists in neutral state. Indeed, NMR data from van der Bergh et al. [32] shows that PFOA adsorbed in the hydrophobic pores of all-silica zeolite Beta is in neutral state, which is in line with our findings.

4. Conclusions

This study provides thermodynamic and kinetic insights into the mechanism of PFOA adsorption from water in all-silica zeolites. Computational screening of all-silica zeolites based on PFOA ideal permeabilities revealed that three zeolites, MTW, VET and GON, are top performers and estimated to exhibit several orders of magnitude better PFOA removal performance compared to zeolite Beta (BEA), which was used as the benchmark material. Free energy analyses revealed that adsorption of PFOA on to the zeolite surface in Orientation I is thermodynamically more favorable than it is in Orientation II; however, when the –CF_3 group of PFOA molecule is adsorbed first on to the zeolite surface (Orientation I) it must overcome an interfacial energy barrier to be completely adsorbed in zeolite pore, whereas, no interfacial energy barrier exists if the –COOH group of PFOA is adsorbed first (Orientation II). This is attributed to the fact that in the latter water attraction between the –COOH group of PFOA and water is insignificant, that is, the adsorption of PFOA in Orientation II is kinetically favored. Probability analyses based on PFOA free energy of surface adsorption showed that PFOA is more likely to be adsorbed in Orientation I on the surface. However, the relative probabilities of finding PFOA molecules in Orientation I and II differ significantly from one zeolite to the other. Given that in MTW, VET and GON, the surface adsorption of PFOA in Orientation II is significantly more probable compared to BEA, the overall PFOA adsorption process is expected to be faster in MTW, VET and GON. Accompanied with thermodynamic and kinetic insights at molecular level, our study shows that zeolite external surfaces and the accompanying interfacial barriers determine the rate limiting step for the PFOA adsorption process. Such detailed understanding would not have been possible by studying the adsorption and diffusion process in the pores only. Furthermore, our findings may also be useful to study the

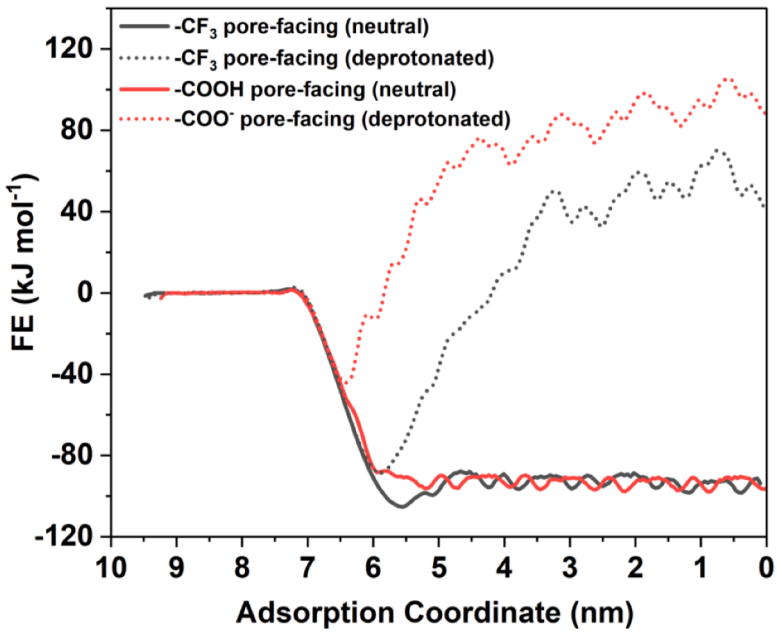

Fig. 6. Comparison of the FE profiles associated with the adsorption of deprotonated and neutral PFOA from water into zeolite BEA.

adsorption of other perfluorinated carboxylic acids from water.

CRediT authorship contribution statement

Mengru Zhang: Investigation, Data curation, Conceptualization, Formal analysis, Visualization, Writing – original draft. **François Sicard:** Writing – review & editing, Methodology. **Turan Selman Erkal:** Software, Methodology. **Geoffrey M. Bowers:** Writing – review & editing. **A. Ozgur Yazaydin:** Project administration, Conceptualization, Methodology, Writing – review & editing.

Declaration of Competing Interest

The authors declare that they have no known competing financial interests or personal relationships that could have appeared to influence the work reported in this paper.

Data availability

Data will be made available on request.

Acknowledgments

The authors acknowledge the use of the University College London (UCL) Myriad High Performance Computing Facility (Myriad@UCL) and associated support services in the completion of this work. The authors are grateful to the UK Materials and Molecular Modelling Hub for computational resources, which is partially funded by EPSRC (EP/P020194/1 and EP/T022213/1). MZ acknowledges support from the UCL-CSC (China Scholarship Council) joint scholarship for PhD studies.

Supplementary materials

Supplementary material associated with this article can be found, in the online version, at doi:10.1016/j.surfin.2023.103271.

References

[1] R. Loos, G. Locoro, S. Comero, S. Contini, D. Schwesig, F. Werres, P. Balsaa, O. Gans, S. Weiss, L. Blaha, M. Bolchi, B.M. Gawlik, Pan-European survey on the occurrence of selected polar organic persistent pollutants in ground water, Water Res. 44 (2010) 4115–4126, https://doi.org/10.1016/j.watres.2010.05.032.

[2] T. Wang, P. Wang, J. Meng, S. Liu, Y. Lu, J.S. Khim, J.P. Giesy, A review of sources, multimedia distribution and health risks of perfluoroalkyl acids (PFAAs) in China, Chemosphere 129 (2015) 87–99, https://doi.org/10.1016/j.chemosphere.2014.09.021.

[3] L.A. Schaider, S.A. Balan, A. Blum, D.Q. Andrews, M.J. Strynar, M.E. Dickinson, D. M. Lunderberg, J.R. Lang, G.F. Peaslee, Fluorinated compounds in U.S. fast food packaging, Environ. Sci. Technol. Lett. 4 (2017) 105–111, https://doi.org/10.1021/acs.estlett.6b00435.

[4] Z. Liu, Y. Lu, T. Wang, P. Wang, Q. Li, A.C. Johnson, S. Sarvajayakesavalu, A. J. Sweetman, Risk assessment and source identification of perfluoroalkyl acids in surface and ground water: spatial distribution around a mega-fluorochemical industrial park, China, Environ. Int. 91 (2016) 69–77, https://doi.org/10.1016/j.envint.2016.02.020.

[5] F. Chirikona, M. Filipovic, S. Ooko, F. Orata, Perfluoroalkyl acids in selected wastewater treatment plants and their discharge load within the Lake Victoria basin in Kenya, Environ. Monit. Assess. 187 (2015) 238, https://doi.org/10.1007/s10661-015-4425-6.

[6] Y. Inoue, N. Hashizume, N. Yakata, H. Murakami, Y. Suzuki, E. Kikushima, M. Otsuka, Unique physicochemical properties of perfluorinated compounds and their bioconcentration in common carp cyprinus carpio L, Arch. Environ. Contam. Toxicol. 62 (2012) 672–680, https://doi.org/10.1007/s00244-011-9730-7.

[7] E. Bizkarguenaga, I. Zabaleta, A. Prieto, L.A. Fernández, O. Zuloaga, Uptake of 8:2 perfluoroalkyl phosphate diester and its degradation products by carrot and lettuce from compost-amended soil, Chemosphere 152 (2016) 309–317, https://doi.org/10.1016/j.chemosphere.2016.02.130.

[8] E.T. Chang, H.O. Adami, P. Boffetta, H.J. Wedner, J.S. Mandel, A critical review of perfluorooctanoate and perfluorooctanesulfonate exposure and immunological health conditions in humans, Crit. Rev. Toxicol. 46 (2016) 279–331, https://doi.org/10.3109/10408444.2015.1122573.

[9] S. Deng, L. Niu, Y. Bei, B. Wang, J. Huang, G. Yu, Adsorption of perfluorinated compounds on aminated rice husk prepared by atom transfer radical polymerization, Chemosphere 91 (2013) 124–130, https://doi.org/10.1016/j.chemosphere.2012.11.015.

[10] J.G. Yu, X.H. Zhao, H. Yang, X.H. Chen, Q. Yang, L.Y. Yu, J.H. Jiang, X.Q. Chen, Aqueous adsorption and removal of organic contaminants by carbon nanotubes, Sci. Total Environ. 482–483 (2014) 241–251, https://doi.org/10.1016/j.scitotenv.2014.02.129.

[11] G.W. Olsen, J.L. Butenhoff, L.R. Zobel, Perfluoroalkyl chemicals and human fetal development: an epidemiologic review with clinical and toxicological perspectives, Reprod. Toxicol. 27 (2009) 212–230, https://doi.org/10.1016/j.reprotox.2009.02.001.

[12] R.A. Dickman, D.S. Aga, A review of recent studies on toxicity, sequestration, and degradation of per- and polyfluoroalkyl substances (PFAS), J. Hazard. Mater. 436 (2022), 129120, https://doi.org/10.1016/j.jhazmat.2022.129120.

[13] S.E. Fenton, A. Ducatman, A. Boobis, J.C. DeWitt, C. Lau, C. Ng, J.S. Smith, S. M. Roberts, Per- and polyfluoroalkyl substance toxicity and human health review: current state of knowledge and strategies for informing future research, Environ. Toxicol. Chem. 40 (2021) 606–630, https://doi.org/10.1002/etc.4890.

[14] S. Gaballah, A. Swank, J.R. Sobus, X.M. Howey, J. Schmid, T. Catron, J. McCord, E. Hines, M. Strynar, T. Tal, Evaluation of developmental toxicity, developmental

neurotoxicity, and tissue dose in zebrafish exposed to GenX and other PFAS, Environ. Health Perspect. 128 (2020), 047005, https://doi.org/10.1289/EHP5843.
[15] G.M. Sinclair, S.M. Long, O.A.H. Jones, What are the effects of PFAS exposure at environmentally relevant concentrations? Chemosphere 258 (2020), 127340 https://doi.org/10.1016/j.chemosphere.2020.127340.
[16] K.H. Harada, H.R. Yang, C.S. Moon, N.N. Hung, T. Hitomi, K. Inoue, T. Niisoe, T. Watanabe, S. Kamiyama, K. Takenaka, M.Y. Kim, K. Watanabe, T. Takasuga, A. Koizumi, Levels of perfluorooctane sulfonate and perfluorooctanoic acid in female serum samples from Japan in 2008, Korea in 1994–2008 and Vietnam in 2007–2008, Chemosphere 79 (2010) 314–319, https://doi.org/10.1016/j.chemosphere.2010.01.027.
[17] Y.J. Lee, M.K. Kim, J. Bae, J.H. Yang, Concentrations of perfluoroalkyl compounds in maternal and umbilical cord sera and birth outcomes in Korea, Chemosphere 90 (2013) 1603–1609, https://doi.org/10.1016/j.chemosphere.2012.08.035.
[18] Drinking water commission of the german ministry of health at the federal environment Agency. Germany, June 21, Provisional evaluation of PFT in drinking water with the guide substances perfluorooctanoic acid (PFOA) and perfluorooctane sulfonate (PFOS) as examples, (2006).
[19] J.L. Domingo, I.E. Jogsten, U. Eriksson, I. Martorell, G. Perelló, M. Nadal, B. van Bavel, Human dietary exposure to perfluoroalkyl substances in Catalonia, Spain, Temporal Trend Food Chem. 135 (2012) 1575–1582, https://doi.org/10.1016/j.foodchem.2012.06.054.
[20] F. Wong, M. Shoeib, A. Katsoyiannis, S. Eckhardt, A. Stohl, P. Bohlin-Nizzetto, H. Li, P. Fellin, Y. Su, H. Hung, Assessing temporal trends and source regions of per- and polyfluoroalkyl substances (PFASs) in air under the Arctic Monitoring and Assessment Programme (AMAP), Atmos. Environ. 172 (2018) 65–73, https://doi.org/10.1016/j.atmosenv.2017.10.028.
[21] Z. Du, S. Deng, Y. Bei, Q. Huang, B. Wang, J. Huang, G. Yu, Adsorption behavior and mechanism of perfluorinated compounds on various adsorbents—a review, J. Hazard. Mater. 274 (2014) 443–454, https://doi.org/10.1016/j.jhazmat.2014.04.038.
[22] M. Trojanowicz, A. Bojanowska-Czajka, I. Bartosiewicz, K. Kulisa, Advanced oxidation/reduction processes treatment for aqueous perfluorooctanoate (PFOA) and perfluorooctanesulfonate (PFOS) – a review of recent advances, Chem. Eng. J. 336 (2018) 170–199, https://doi.org/10.1016/j.cej.2017.10.153.
[23] P. Li, D. Zhi, X. Zhang, H. Zhu, Z. Li, Y. Peng, Y. He, L. Luo, X. Rong, Y. Zhou, Research progress on the removal of hazardous perfluorochemicals: a review, J. Environ. Manage. 250 (2019), 109488, https://doi.org/10.1016/j.jenvman.2019.109488.
[24] L. Liu, Y. Liu, B. Gao, R. Ji, C. Li, S. Wang, Removal of perfluorooctanoic acid (PFOA) and perfluorooctane sulfonate (PFOS) from water by carbonaceous nanomaterials: a review, Crit. Rev. Environ. Sci. Technol. 50 (2020) 2379–2414, https://doi.org/10.1080/10643389.2019.1700751.
[25] Y. Yang, W. Ji, X. Li, Z. Zheng, F. Bi, M. Yang, J. Xu, X. Zhang, Insights into the degradation mechanism of perfluorooctanoic acid under visible-light irradiation through fabricating flower-shaped Bi5O7I/ZnO n-n heterojunction microspheres, Chem. Eng. J. 420 (2021), 129934, https://doi.org/10.1016/j.cej.2021.129934.
[26] Y. Yang, Z. Zheng, W. Ji, J. Xu, X. Zhang, Insights to perfluorooctanoic acid adsorption micro-mechanism over Fe-based metal organic frameworks: combining computational calculation with response surface methodology, J. Hazard. Mater. 395 (2020), 122686, https://doi.org/10.1016/j.jhazmat.2020.122686.
[27] Y. Yang, Z. Zheng, M. Yang, J. Chen, C. Li, C. Zhang, X. Zhang, In-situ fabrication of a spherical-shaped Zn-Al hydrotalcite with BiOCl and study on its enhanced photocatalytic mechanism for perfluorooctanoic acid removal performed with a response surface methodology, J. Hazard. Mater. 399 (2020), 123070, https://doi.org/10.1016/j.jhazmat.2020.123070.
[28] V. Ochoa-Herrera, R. Sierra-Alvarez, Removal of perfluorinated surfactants by sorption onto granular activated carbon, zeolite and sludge, Chemosphere 72 (2008) 1588–1593, https://doi.org/10.1016/j.chemosphere.2008.04.029.
[29] P. Punyapalakul, K. Suksomboon, P. Prarat, S. Khaodhiar, Effects of surface functional groups and porous structures on adsorption and recovery of perfluorinated compounds by inorganic porous silicas, Sep. Sci. Technol. 48 (2013) 775–788, https://doi.org/10.1080/01496395.2012.710888.
[30] M. Sörengård, E. Östblom, S. Köhler, L. Ahrens, Adsorption behavior of per- and polyfluoroalkyl substances (PFASs) to 44 inorganic and organic sorbents and use of dyes as proxies for PFAS sorption, J. Environ. Chem. Eng. 8 (2020), 103744, https://doi.org/10.1016/j.jece.2020.103744.
[31] M. Mancinelli, C. Stevanin, M. Ardit, T. Chenet, L. Pasti, A. Martucci, PFAS as emerging pollutants in the environment: a challenge with FAU type and silver-FAU exchanged zeolites for their removal from water, J. Environ. Chem. Eng. 10 (2022), 108026, https://doi.org/10.1016/j.jece.2022.108026.
[32] M. Van den Bergh, A. Krajnc, S. Voorspoels, S.R. Tavares, S. Mullens, I. Beurroies, G. Maurin, G. Mali, D.E. De Vos, Highly selective removal of perfluorinated contaminants by adsorption on all-silica zeolite beta, Angew. Chem. 132 (2020) 14190–14194, https://doi.org/10.1002/ange.202002953.
[33] Md.S. Hossain, T.D. Stuart, B.V. Ramarao, C.C. VanLeuven, M. Wriedt, D. Kiemle, M. Satchwell, D. Kumar, Investigation into cationic surfactants and polyelectrolyte-coated β-zeolites for rapid and high-capacity adsorption of short- and long-chain PFAS, Ind. Eng. Chem. Res. 62 (2023) 8373–8384, https://doi.org/10.1021/acs.iecr.3c00468.
[34] G.M. Torrie, J.P. Valleau, Nonphysical sampling distributions in Monte Carlo free-energy estimation: umbrella sampling, J. Comput. Phys. 23 (1977) 187–199, https://doi.org/10.1016/0021-9991(77)90121-8.
[35] A. Laio, M. Parrinello, Escaping free-energy minima, Proc. Natl. Acad. Sci. 99 (2002) 12562–12566, https://doi.org/10.1073/pnas.202427399.
[36] M.F. Richter, B.S. Drown, A.P. Riley, A. Garcia, T. Shirai, R.L. Svec, P. J. Hergenrother, Predictive compound accumulation rules yield a broad-spectrum antibiotic, Nature 545 (2017) 299–304, https://doi.org/10.1038/nature22308.
[37] E. Darve, A. Pohorille, Calculating free energies using average force, J. Chem. Phys. 115 (2001) 9169–9183, https://doi.org/10.1063/1.1410978.
[38] P. Pongprayoon, O. Beckstein, C.L. Wee, M.S.P. Sansom, Simulations of anion transport through OprP reveal the molecular basis for high affinity and selectivity for phosphate, Proc. Natl. Acad. Sci. 106 (2009) 21614–21618, https://doi.org/10.1073/pnas.0907315106.
[39] K. Atkovska, J.S. Hub, Energetics and mechanism of anion permeation across formate-nitrite transporters, Sci. Rep. 7 (2017) 12027, https://doi.org/10.1038/s41598-017-11437-0.
[40] F. Sicard, T. Bui, D. Monteiro, Q. Lan, M. Ceglio, C. Burress, A. Striolo, Emergent properties of antiagglomerant films control methane transport: implications for hydrate management, Langmuir 34 (2018) 9701–9710, https://doi.org/10.1021/acs.langmuir.8b01366.
[41] J.S. Hub, B.L. de Groot, D. van der Spoel, g_wham—a free weighted histogram analysis implementation including robust error and autocorrelation estimates, J. Chem. Theory Comput. 6 (2010) 3713–3720, https://doi.org/10.1021/ct100494z.
[42] C. Baerlocher, LB. McCusker, Database of zeolite structures, (2017). http://www.iza-structure.org/databases/.
[43] L. Sarkisov, R. Bueno-Perez, M. Sutharson, D. Fairen-Jimenez, Materials informatics with PoreBlazer v4.0 and the CSD MOF database, Chem. Mater. 32 (2020) 9849–9867, https://doi.org/10.1021/acs.chemmater.0c03575.
[44] G. Kamath, F. Cao, J.J. Potoff, An improved force field for the prediction of the vapor−liquid equilibria for carboxylic acids, J. Phys. Chem. B 108 (2004) 14130–14136, https://doi.org/10.1021/jp048581s.
[45] J.M. Stubbs, J.J. Potoff, J.I. Siepmann, Transferable potentials for phase equilibria. 6. United-atom description for ethers, glycols, ketones, and aldehydes, J. Phys. Chem. B. 108 (2004) 17596–17605, https://doi.org/10.1021/jp049459w.
[46] L. Zhang, J.I. Siepmann, Pressure dependence of the vapor−liquid−liquid phase behavior in ternary mixtures consisting of *n* -Alkanes, *n* -Perfluoroalkanes, and carbon dioxide, J. Phys. Chem. B 109 (2005) 2911–2919, https://doi.org/10.1021/jp0482114.
[47] J.J. Potoff, D.A. Bernard-Brunel, Mie potentials for phase equilibria calculations: application to alkanes and perfluoroalkanes, J. Phys. Chem. B 113 (2009) 14725–14731, https://doi.org/10.1021/jp9072137.
[48] T.S. Erkal, N. Shamsuddin, S. Kirmizialtin, A.O. Yazaydin, Computational investigation of structure–function relationship in fluorine-functionalized MOFs for PFOA capture from water, J. Phys. Chem. C 127 (2023) 3204–3216, https://doi.org/10.1021/acs.jpcc.2c07737.
[49] H.J.C. Berendsen, J.R. Grigera, T.P. Straatsma, The missing term in effective pair potentials, J. Phys. Chem. 91 (1987) 6269–6271, https://doi.org/10.1021/j100308a038.
[50] D. Frenkel, B. Smit, Understanding Molecular simulation: from Algorithms to Applications, 2nd ed., Academic Press, San Diego, 2002.
[51] A.L. Myers, P.A. Monson, Adsorption in porous materials at high pressure: theory and experiment, Langmuir 18 (2002) 10261–10273, https://doi.org/10.1021/la026399h.
[52] J.M. Castillo, D. Dubbeldam, T.J.H. Vlugt, B. Smit, S. Calero, Evaluation of various water models for simulation of adsorption in hydrophobic zeolites, Mol. Simul. 35 (2009) 1067–1076, https://doi.org/10.1080/08927020902865923.
[53] D. Dubbeldam, S. Calero, D.E. Ellis, R.Q. Snurr, RASPA: molecular simulation software for adsorption and diffusion in flexible nanoporous materials, Mol. Simul. 42 (2016) 81–101, https://doi.org/10.1080/08927022.2015.1010082.
[54] M.P. Allen, D.J. Tildesley, Computer Simulation of Liquids, 2nd edition, Oxford University Press, Oxford, United Kingdom, 2017.
[55] A. Einstein, The motion of elements suspended in static liquids as claimed in the molecular kinetic theory of heat, Ann. Phys. 17 (1905) 549–560.
[56] D.J. Evans, B.L. Holian, The Nose–hoover thermostat, J. Chem. Phys. 83 (1985) 4069–4074, https://doi.org/10.1063/1.449071.
[57] M.J. Abraham, T. Murtola, R. Schulz, S. Páll, J.C. Smith, B. Hess, E. Lindahl, GROMACS: high performance molecular simulations through multi-level parallelism from laptops to supercomputers, SoftwareX 1–2 (2015) 19–25, https://doi.org/10.1016/j.softx.2015.06.001.
[58] L. Vierke, U. Berger, I.T. Cousins, Estimation of the acid dissociation constant of perfluoroalkyl carboxylic acids through an experimental investigation of their water-to-air transport, Environ. Sci. Technol. 47 (2013) 11032–11039, https://doi.org/10.1021/es402691z.
[59] J.L. López-Fontán, F. Sarmiento, P.C. Schulz, The aggregation of sodium perfluorooctanoate in water, Colloid Polym. Sci. 283 (2005) 862–871, https://doi.org/10.1007/s00396-004-1228-7.
[60] N.O. Brace, Long chain alkanoic and alkenoic acids with perfluoroalkyl terminal segments [1], J. Org. Chem. 27 (1962) 4491–4498, https://doi.org/10.1021/jo01059a090.
[61] D.C. Burns, D.A. Ellis, H. Li, C.J. McMurdo, E. Webster, Experimental p K_a determination for perfluorooctanoic acid (PFOA) and the potential impact of p K_a Concentration dependence on laboratory-measured partitioning phenomena and environmental modeling, Environ. Sci. Technol. 42 (2008) 9283–9288, https://doi.org/10.1021/es802047v.
[62] S. Rayne, K. Forest, K.J. Friesen, Computational approaches may underestimate pK *a* values of longer-chain perfluorinated carboxylic acids: implications for assessing environmental and biological effects, J. Environ. Sci. Health Part A 44 (2009) 317–326, https://doi.org/10.1080/10934520802659620.

[63] N. Loganathan, A.K. Wilson, Adsorption, structure, and dynamics of short- and long-chain PFAS molecules in kaolinite: molecular-level insights, Environ. Sci. Technol. 56 (2022) 8043–8052, https://doi.org/10.1021/acs.est.2c01054.
[64] J.A.R. Willemsen, I.C. Bourg, Molecular dynamics simulation of the adsorption of per- and polyfluoroalkyl substances (PFASs) on smectite clay, J. Colloid Interface Sci. 585 (2021) 337–346, https://doi.org/10.1016/j.jcis.2020.11.071.
[65] A. Choudhary, D. Dong, M. Tsianou, P. Alexandridis, D. Bedrov, Adsorption mechanism of perfluorooctanoate on cyclodextrin-based polymers: probing the synergy of electrostatic and hydrophobic interactions with molecular dynamics simulations, ACS Mater. Lett. 4 (2022) 853–859, https://doi.org/10.1021/acsmaterialslett.2c00168.
[66] J.G. Wijmans, R.W. Baker, The solution-diffusion model: a review, J. Membr. Sci. 107 (1995) 1–21, https://doi.org/10.1016/0376-7388(95)00102-I.
[67] C.H. Lee, Theory of reverse osmosis and some other membrane permeation operations, J. Appl. Polym. Sci. 19 (1975) 83–95, https://doi.org/10.1002/app.1975.070190107.
[68] H. Eyring, The activated complex in chemical reactions, J. Chem. Phys. 3 (1935) 107–115, https://doi.org/10.1063/1.1749604.
[69] P.W. Atkins, J. De Paula, J. Keeler, Atkins' Physical chemistry, 11th ed., Oxford University Press, Oxford, United Kingdom; New York, NY, 2018.